

1

Introduction

We begin this book with the definition and characterization of single-photon sources: How are they different from standard light sources, and how do they work? We will then discuss the basic motivation for generation and detection of single photons: When do we need single photons in place of standard laser emission? Over the past ten years, on-demand single-photon generation has been realized in numerous physical systems including atoms, ions, molecules, solid-state quantum dots, impurities and defects, and superconducting circuits. We will conclude this introductory chapter with a historical review of these demonstrations.

1.1

Definition and Characteristics of Single-Photon Sources

This book describes devices designed to emit *single* photons at designated time instances. Before describing how such a device might be constructed and operated, let us define exactly what we mean by a source of single photons. The following presentation closely follows one given by the authors in [1].

A single-photon source is quite different from a classical light source such as a laser, a light emitting diode or a parametric amplifier/oscillator where the number of photons or photon pairs per pulse varies randomly, usually following a Poisson distribution. Nevertheless, a realistic single-photon source will never be perfect and will, on occasion, emit zero or multiple photons. Therefore, the distinction between a classical photon source and a realistic single-photon source requires quantitative measures based on photon statistics. From the viewpoint of quantum information system applications, other characteristics are also important. Some of the most important parameters describing a single-photon source are:

1. The second-order coherence function $g_0^{(2)}$ [2] which places an upper bound on the two or multi-photon probability per pulse, $p_m = p(n \geq 2) \leq (1/2)g_0^{(2)}\langle n \rangle^2$, where $\langle n \rangle$ is the average photon number per pulse. A photon source with $\langle n \rangle = 1$ and with, $g_0^{(2)} = 1$, $g_0^{(2)} < 1$, or $g_0^{(2)} = 0$ is called a Poisson, sub-Poisson or ideal single-photon source, respectively. Since a realistic single-

photon source has $0 < g_0^{(2)} < 1$, it is a sub-Poisson photon source operating in the regime of $\langle n \rangle \lesssim 1$. When a single-photon source is used in quantum key distribution systems, the robustness against a specific eavesdropping attack, called the photon number splitting attack, requires a small value of $g_0^{(2)}$ [3].

2. An external quantum efficiency η_{total} , which defines an overall out-coupling efficiency of internally generated single photons into a desired single waveguide mode.
3. The maximum repetition frequency f_{max} of single-photon generation, which determines an upper bound on the clock frequency of a system. These two parameters, η_{total} and f_{max} , must be reasonably high for practical applications. In the case of a laser, the stimulated emission of photons enhances these parameters. For a single-photon source, however, stimulated emission is not an option and we need a new trick to achieve high values of η_{total} and f_{max} . One of the most useful techniques available for this purpose is to use cavity quantum electrodynamical effects [4] to enhance spontaneous emission.
4. The overlap $F(\Delta t = 0) = \langle |\int dt x(t)\gamma^*(t)|^2 \rangle$ between two single-photon wave functions defined by $|\psi\rangle_{12} = \int dt \int dt' x(t)\gamma(t' - \Delta t)\hat{a}_1^\dagger(t)\hat{a}_2^\dagger(t')|0\rangle_1|0\rangle_2$, where $\hat{a}_i^\dagger(t)$ is the photon creation operator at time t for mode i , $x(t)$ and $\gamma(t)$ define the photon waveforms, $|0\rangle_i$ is the vacuum state, and Δt is the relative delay between the two photons [5, 6]. This overlap can be computed either in the space-time or momentum-frequency domains, and an ensemble average is taken over the quantum states generated by the source. To use a single-photon source for quantum information systems such as a linear-optics Bell state analyzer, entangled photon-pair generation, quantum teleportation, generation of entangled states in remote memories, and linear optics quantum computation, single photons must be identical quantum particles with $F(0) = 1$. However, a realistic single-photon source has a finite timing jitter and dephasing in the generated electromagnetic field, which reduces $F(0)$ below one. We shall also refer to F as the photon ‘indistinguishability’.
5. An emission wavelength uncertainty, $\Delta\lambda$, in different single-photon sources. When a single-photon source is used in a large-scale photonic system, massively parallel generation of single photons is needed. In such a case, the emission wavelength of single-photon sources must be identical or at least the inhomogeneous broadening $\Delta\lambda$ must be much smaller than the intrinsic linewidth.

1.2

Single-Photon Generation with Atom-Like Systems

The type of single-photon source we will be studying in this book uses a single atom or atom-like system that is induced through optical or electrical excitation to emit a single photon. In the case of optical excitation, we start out with an incoming laser pulse in which the photon number follows a Poisson distribution,

$$p_n = \frac{\mu^n}{n!} e^{-\mu} \quad (1.1)$$

where p_n is the probability that the pulse contains n photons, and $\mu = \langle n \rangle$ is the mean photon number. The purpose of the atom is then to convert this into an output pulse containing exactly one photon, preferably at another frequency, so that in the output field $p_1 = 1$, and $p_{n \neq 1} = 0$. In this sense, the atom acts as a nonlinear filter.

Most experimentally demonstrated single-photon sources based on optically excited atom-like systems in solids have used energy-level structures with at least three discrete states. In the simplest and most commonly used scheme shown in Figure 1.1a, an external pump source excites the system from state $|b\rangle$ to state $|r\rangle$, which is followed by rapid relaxation to state $|a\rangle$ through emission of phonons, for example. The system then emits a single photon by spontaneous emission as it transitions from state $|a\rangle$ to state $|b\rangle$. We refer to this excitation process as “incoherent” pumping. If the quantum system is placed inside of an optical microcavity, the cavity field is resonantly coupled to the atomic transition between the $|a\rangle$ and $|b\rangle$ states. In the case of an electrically neutral quantum dot, the $|b\rangle$, $|a\rangle$ and $|r\rangle$ states may correspond to the crystal ground state (empty quantum dot), a “single-exciton” state with one electron–hole pair at the $1e-1h$ transition, and an excited single-exciton state with one electron–hole pair at the $2e-2h$ transition, respectively. Here, $1e$ and $2e$ are the lowest and the first excited conduction-band electron states in a quantum dot, while $1h$ and $2h$ are the lowest and the first excited heavy-hole valence-band states, respectively.

In theory, better performance is possible in coherent excitation schemes. One such scheme involves a Raman scattering process in a three-level system, as shown in Figure 1.1b. This scheme requires two metastable ground states $|g\rangle$ and $|e\rangle$ which can be physically realized, for instance, by the Zeeman splitting of a single trapped electron inside a quantum dot. These metastable states are optically coupled to an excited state $|r\rangle$ which, in the quantum-dot case, would correspond to a charged-exciton (or trion) state having two electrons and one hole. An optical microcavity resonantly coupled to the $r-e$ transition greatly improves the performance of this scheme. One also has the option of detuning the excitation laser from the $g-r$ transition, which may provide some advantage with respect to excited-state dephasing processes. These issues are discussed in more detail in Chapters 2, 3, and 4.

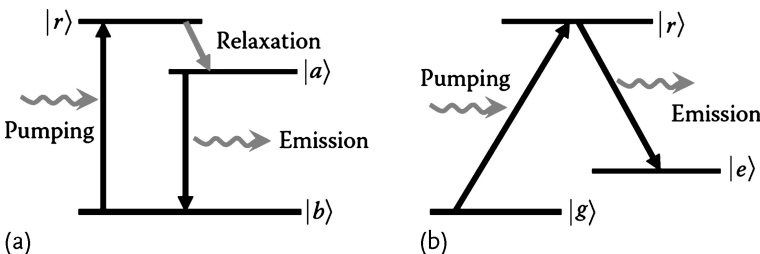


Figure 1.1 Three-level schemes used for generating single photons. (a) “Incoherent” excitation scheme for generating single photons by spontaneous emission. (b) Coherent excitation scheme for generating single photons by Raman scattering.

Let us now introduce some physical parameters important in describing a single-photon source. Suppose we have an atomic dipole transition coupled to a single mode of an optical microcavity as shown in Figure 1.2. The coupling rate between the atom and a single photon in the cavity mode is given by the so-called vacuum Rabi frequency [7],

$$g_0 = \frac{\mu}{\hbar} \sqrt{\frac{\hbar \omega_c}{2\epsilon V}} \quad (1.2)$$

where μ is the dipole moment, ω_c is the frequency of the cavity resonance, $\epsilon = \epsilon_0 n^2$ is the permittivity of the semiconductor at the optical frequency, n is the refractive index, and V is the cavity mode volume. For the present discussion, we have assumed that the dipole is located at the cavity field maximum and that the dipole is perfectly aligned with the electric field. The spontaneous emission rate for the $a \rightarrow b$ transition in the bulk material (without the cavity) is obtained from the Weisskopf–Wigner approximation as [7]

$$\Gamma = \frac{n \omega_a^3 \mu^2}{3\pi \epsilon_0 \hbar c^3} \quad (1.3)$$

where ω_a is the frequency of the atomic dipole transition. It is also convenient to define a dimensionless oscillator strength,

$$f_{\text{osc}} = \frac{\Gamma}{3\Gamma_{\text{ceo}}} = \frac{1}{(4\pi K)^2} \left(\frac{\lambda}{n}\right)^3 \omega_a \Gamma \quad (1.4)$$

Here, $K = e/\sqrt{4\epsilon m_e}$, where e and m_e are the electron charge and mass, λ is the wavelength in vacuum, and $\Gamma_{\text{ceo}} = n \omega_a^2 e^2 / (6\pi \epsilon_0 m_e c^3)$ is the spontaneous emission rate for a classical electron oscillator [8]. For the cavity, we can then re-write the vacuum Rabi frequency as

$$g_0 = K \sqrt{3f_{\text{osc}}/V} \quad (1.5)$$

We note that if n photons are present in the cavity, g_0 as defined above is replaced by $g_0 \sqrt{1+n}$. This quantity is equal to one-half of the Rabi frequency Ω that describes an atomic transition driven by a “classical” field.

The parameter V , which determines the atom-cavity coupling strength, is the mode volume of the cavity, defined as

$$V = \frac{\int \int \int \epsilon(\mathbf{r}) |E(\mathbf{r})|^2 d^3 \mathbf{r}}{\max(\epsilon(\mathbf{r}) |E(\mathbf{r})|^2)} \quad (1.6)$$

For the maximum possible interaction between a cavity photon and an atomic dipole, the electric field of a single photon should be as large as possible at the location of the atom. This occurs when we confine the photon to the smallest possible space. Another important parameter is the rate at which photons leak out of the cavity. This is given by $\kappa = \kappa_C + \kappa_L$, where κ_C is the rate at which photons couple

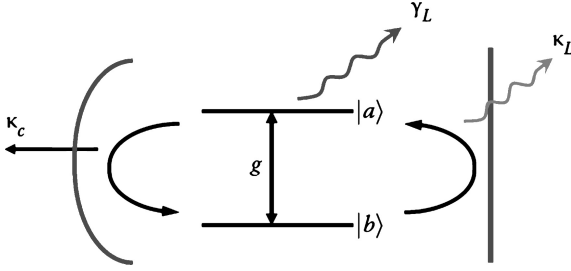


Figure 1.2 A single “atom”-cavity system and physical parameters.

to a down-stream optical mode and κ_L is the rate at which photons are lost to other spurious modes or absorption inside the cavity. The parameter κ determines the length of time over which the atom and cavity photon can interact. This is related to the quality factor of the cavity, defined as $Q = \omega_{\text{cav}}/\kappa$, where ω_{cav} is the cavity resonance frequency in angular units. The small size of semiconductor micro-cavities makes them subject to surface defects and interface roughness, which prevents Q from being as high as in larger cavities. The ratio κ_C/κ determines the coupling efficiency between a cavity and an external optical channel. For single-photon generation and quantum networking, the ratio κ_C/κ should be close to one, a situation referred to as “over-coupling.” This ensures that photons escaping from the cavity are collected in the down-stream optical mode. Finally, the parameter γ_L is the spontaneous emission rate of photons directly into “leaky” modes outside of the cavity. We usually expect $\gamma_L \sim \Gamma$, although in semiconductor microcavity structures such as photonic crystals, the two quantities can differ significantly.

As explained in Chapter 2, if the atom and cavity are exactly on resonance, considering only two atomic levels, the eigenfrequencies of the coupled atom-cavity system are

$$\omega_{\pm} = \omega_a - i(\kappa + \gamma_L)/4 \pm \sqrt{g_0^2 - (\kappa - \gamma_L)^2/16} \quad (1.7)$$

When $g_0 > |\kappa - \gamma_L|/4$, the system shows a normal mode splitting into two dressed states separated by twice the vacuum Rabi frequency $2g_0$. This is known as the strong-coupling regime, and corresponds physically to a situation in which energy can oscillate back and forth between the atom and the cavity before it escapes from the system, either through spontaneous emission by the atom into “leaky” modes, or by escape of the photon from the cavity. For single-photon generation, it is generally *not* helpful for the system to be far into the strong coupling regime. In the opposite limit, for $g, \gamma_L \ll \kappa$, the + solution of Eq. (1.7) is $\omega_+ = \omega_a - i(\gamma_L/2)(1 + C)$, where C is the “cooperativity parameter” given by

$$C = \frac{4g_0^2}{\kappa\gamma_L} \approx 3/4\pi^2 \times (\lambda/n)^3 \times Q/V \quad (1.8)$$

where in the second expression we have assumed $\gamma_L = \Gamma$. This parameter indicates the degree to which the spontaneous emission rate is enhanced by the cavity.

Semiconductor microcavity systems offer a key advantage in achieving high values of C compared with larger cavities that might be used with trapped atoms or ions.

The total efficiency to collect a single photon can be expressed as

$$\eta_{\text{total}} \approx \left(\frac{C}{C+1} \right) \left(\frac{\kappa_C}{\kappa_C + \kappa_L} \right) \quad (1.9)$$

where the first term represents loss through spontaneous emission directly into leaky modes outside of the cavity, and the second term represents loss of the cavity photon to modes other than the desired one.

1.3

Applications of Single Photons

1.3.1

Quantum Erasure through Optical Interference

A quantum state of light from an ideal laser operating well above threshold is close to a coherent state [9, 10], except for the fact that the laser emission has random-walk phase diffusion due to the lack of a phase-restoring force in such a phase-insensitive amplifying system [11]. If the measurement time interval or the time delay in an interferometer is much shorter than the phase diffusion time (or coherence time) of the laser, phase diffusion can be neglected, and the laser emission is indistinguishable from a coherent state.

Some of the most successful applications for lasers have been those based on optical interferometry, including optical precision measurement, imaging, and lithography. As an example, Figure 1.3 shows a Mach-Zehnder interferometer in which the phase shift in the lower arm can be scanned by angle $\Delta\theta$. In this way, an additional small phase shift $\Delta\phi$ can be detected via the shift of the interference fringe pattern. A remarkable feature of this instrument is that complete interference with perfect visibility is obtained no matter how large the optical losses are in the two arms, provided the losses are equal. This is straightforward to show using classical electromagnetic theory because a bright laser is a good approximation of a clas-

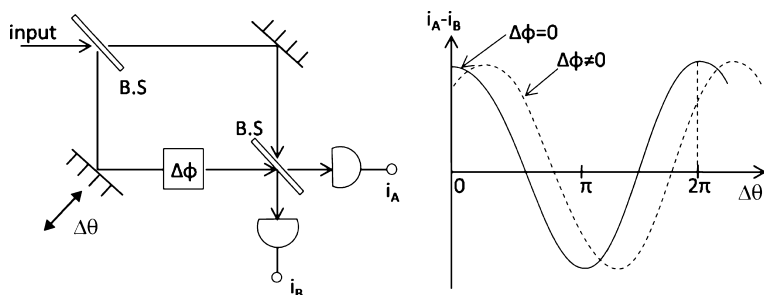


Figure 1.3 A Mach-Zehnder interferometer for differential phase detection.

sical field. However, perfect interference will occur for *any* quantum state, even a Fock (photon number) state containing exactly one photon. This may seem surprising given that a single-photon state has maximal uncertainty of the classical “phase” variable. For quantum states, the preservation of perfect interference can be viewed as a consequence of the famous “quantum erasure” effect which is naturally implemented by the final beam-splitter in this instrument. To understand quantum erasure, let us consider the following thought experiments.

Experiment 1 If we could observe a photon propagating in one of the two arms by means of a *quantum non-demolition* measurement, the interference pattern would disappear as shown in Figure 1.4. A non-demolition measurement detects the presence of the photon while allowing it to pass through. Such a measurement could be implemented by inserting a Kerr nonlinear medium and interacting the photon with a probe beam [12]. The interference is destroyed in this case because it is possible from the measurement to know whether a particular photon that exits from the final beam-splitter traveled through the upper or lower arm. This is called a which-path measurement.

Experiment 2 If we place a strong absorbing medium in one of the two arms, the interference pattern would also disappear, as shown in Figure 1.5. This is because each detected photon almost certainly propagated through the lower arm without the absorber. The absorber effectively realizes a which-path measurement.

Experiment 3 If we place a second absorber in the other arm and balance the two attenuation constants, we can recover complete interference with perfect visibility as shown in Figure 1.6. Once again, we cannot tell which path each detected photon took through the interferometer. Of course, photons that are lost in the absorber can, in principle, be measured by the environment, but these photons do not contribute to the signal measured at the interferometer output. Measurement of a photon at the interferometer output *post-selects* a situation in which a photon was not lost in either absorber, and no information has been leaked to the environment about which path was taken.

Every optical interferometric instrument is based on this remarkable effect of quantum erasure. By adjusting the two attenuation constants to be equal, a perfect interference pattern can be obtained in spite of a highly dissipative environment, and thus various practical applications become possible.

A Mach–Zehnder interferometer can be operated with any input state of light including a coherent state, a photon number state and even a thermal state. For a coherent state, the measurement sensitivity for a small phase shift $\Delta\phi$ is determined by the total number N of detected photons in a measurement time interval, that is, $\Delta\phi \sim \frac{1}{\sqrt{2N}}$ [13]. As one might expect, the measurement sensitivity improves with increasing photon number. Why, then, would you ever want to send a *single* photon through an interferometer? One reason, which we shall discuss next, might be to keep the measurement result of $\Delta\phi$ secret. If you want to be the only person who knows $\Delta\phi$, you must choose one and only one particular quantum state of light, which is the single-photon state.

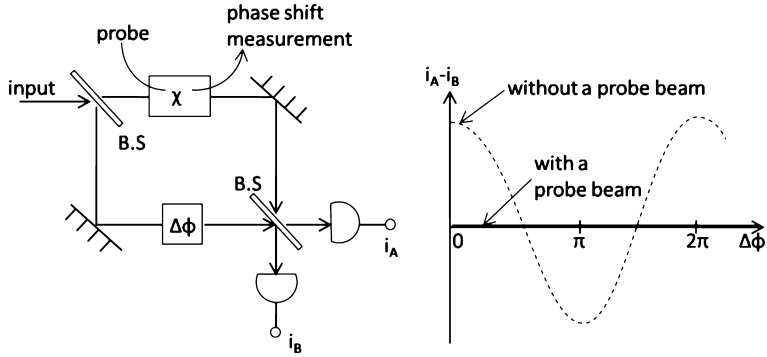


Figure 1.4 A Mach-Zehnder interferometer with a quantum non-demolition detector of photons in one arm [12].

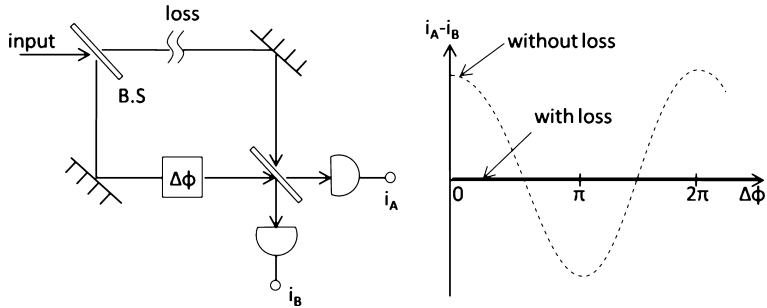


Figure 1.5 A Mach-Zehnder interferometer with an attenuator in one arm.

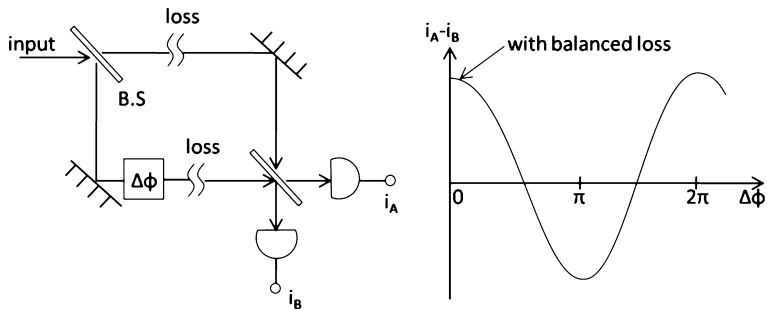


Figure 1.6 A Mach-Zehnder interferometer with balanced attenuators in two arms.

1.3.2

Secure Communication

Suppose we have an interferometer as in Figure 1.3, but the phase shifter represented by $\Delta\phi$ is close to the first beam-splitter and is under the control of a sender,

Alice. If Alice sends only a single photon through the interferometer, and it is detected at the interferometer output by a receiver, Bob, then Alice and Bob can be sure that there is no other photon carrying information about $\Delta\phi$ that could have been lost to someone. The gained information is secure and can be used as a secret key for cryptographic communication. Of course, each detected single photon can provide only one bit of classical information, that is, $\Delta\phi = 0$ or π , in this case. This is the basic principle of quantum key distribution in quantum cryptography. In the particular protocol referred to as BB84 [14], Alice randomly modulates $\Delta\phi$ between 0 and π or between $-\frac{\pi}{2}$ and $\frac{\pi}{2}$. The two partial waves represented by the interferometer in Figure 1.3 need not be spatially separated modes, but may instead be two orthogonally polarized modes in the same space. Bob recombines the two partial waves of the single photon on a 50–50 beam-splitter (or with a waveplate in the polarization implementation) with or without an additional $\frac{\pi}{2}$ phase shift on the encoded partial wave, to decode the phase information. For those instances in which Alice chose a 0– π phase base and Bob did not add an additional $\frac{\pi}{2}$ phase shift, or vice versa, Alice and Bob can share a secret bit without an eavesdropper’s attack being possible even in principle, no matter how large the optical loss is. Whenever Bob detects a single photon, the lossy transmission line did not absorb that particular single photon, and thus no information was leaked to anyone else.

1.3.3

Creating Entanglement between Matter Qubits

Let us next consider a Mach–Zehnder interferometer with two phase shifters. We assume the two phase shifters are quantum mechanical objects and their phase shifts are prepared to be simultaneously 0 and π with equal probability amplitudes. Figure 1.7 shows an experimental system which could, in principle, realize this situation. A single atom with a three-level lambda configuration with states $|g\rangle$, $|e\rangle$, and $|r\rangle$ is put into a cavity. The cavity is nearly resonant with the e – r transition with

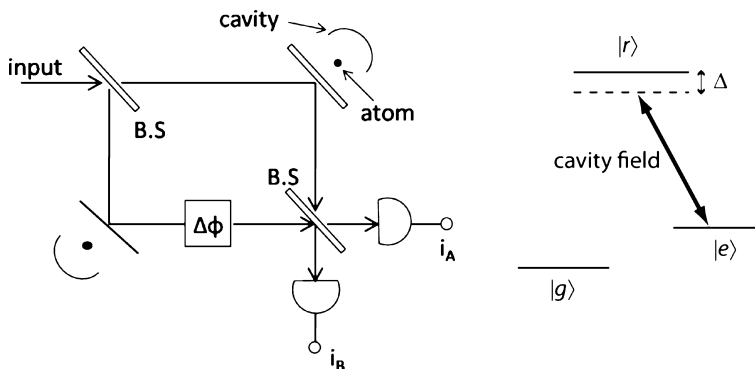


Figure 1.7 A Mach–Zehnder interferometer with two quantum phase shifters and probed by a single photon [88].

cooperativity parameter $C \gg 1$. If a narrowband incident optical field is resonant with the cavity, it will acquire a π phase shift (relative to the empty-cavity situation) if the atom is in state $|e\rangle$, and zero phase shift if the atom is in state $|g\rangle$.

Suppose the atoms are initially prepared in superposition states,

$$|\phi\rangle_{\text{atom}} = \frac{1}{\sqrt{2}}(|g\rangle + |e\rangle)_1 \otimes \frac{1}{\sqrt{2}}(|g\rangle + |e\rangle)_2 \quad (1.10)$$

and then a single photon is sent through the interferometer. If a single photon is detected at one output port (A), we can conclude that the two phase shifters are in the same states (either in $|0\rangle_1|0\rangle_2$ or $|\pi\rangle_1|\pi\rangle_2$) so that the post-selected atomic state is in an EPR-Bell state,

$$|\phi\rangle_{\text{atom}} = \frac{1}{\sqrt{2}}(|g\rangle_1|g\rangle_2 + |e\rangle_1|e\rangle_2) \quad (1.11)$$

Similarly, if a single photon is detected at the other output port (B), we can conclude the atomic state is in another EPR-Bell state:

$$|\phi\rangle_{\text{atom}} = \frac{1}{\sqrt{2}}(|g\rangle_1|e\rangle_2 + |e\rangle_1|g\rangle_2) \quad (1.12)$$

In this way, we can generate an EPR-Bell state of atomic qubits by sending and detecting a single photon. The same scheme could also be used with a coherent state containing many photons instead of a single-photon state. In that case, it is advantageous to use a detuning Δ between the cavity resonance and the e - r transition, as indicated in Figure 1.7. However, if finite loss is present in the interferometer, the superposition of the atomic state collapses to either $|g\rangle$ or $|e\rangle$ via hypothetical measurements performed on the lost photons. There is no need to actually perform such a measurement since the theoretical possibility of such a measurement is enough to collapse a quantum state. The use of a single photon eliminates even such a theoretical possibility. When the single photon is lost, nothing is detected, so the scheme fails. However, since this failure is known, one can “repeat until success” if desired.

The Mach–Zehnder interferometer shown in Figure 1.7 has one disadvantage. If the two quantum memories are separated by a long distance, which is indeed the case for long-distance quantum communication systems, the two arms of the Mach–Zehnder interferometer would be independent optical fibers with random phase fluctuations. It is impractical to stabilize the differential phase in this case. Figure 1.8 shows another scheme that uses differential phase detection to circumvent this problem [15]. A single photon is split into a superposition of two separate pulses, a probe and a reference, by a 50–50 beam-splitter. Only the probe pulse senses the phase shifts of the two atom-cavity systems, while the reference pulse, propagating with a short delay from the probe and acquiring exactly the same phase fluctuation in the channel, does not interact with the two atom-cavity systems. Thus, an optical homodyne detection signal generated by the beat note between the probe and reference pulses automatically cancels the fiber phase fluctuations.

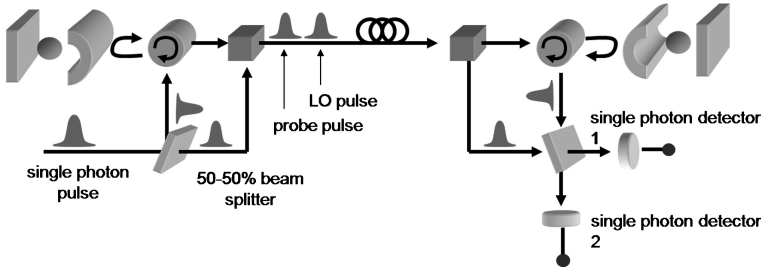


Figure 1.8 A scheme for generation of atomic entangled states by differential phase detection of single photons, similar to [15]. Kaoru Sanaka.

We have not yet discussed the physical mechanism by which the atom-cavity system applies a phase shift to the reflected single-photon state in the above schemes. One way to think of it is that, in response to the excitation field, the atom generates its own field which is superimposed on the field that is directly reflected by the cavity. The total field then has a shifted phase. However, single-photon states spontaneously emitted by atoms can also be used by themselves to generate entanglement through quantum erasure. Numerous schemes have now been proposed for this, starting with a scheme proposed by Cabrillo *et al.* based on Raman scattering [16]. Many of these schemes suffer from the phase stabilization problem discussed above and may only be suitable for communication over a short distance, perhaps within a single temperature-stabilized chip.

Figure 1.9 shows a possible experimental scheme based on quantum interference between two indistinguishable single photons produced by spontaneous emission that circumvents the fiber phase fluctuation problem [17]. In this scheme, the two atoms are simultaneously prepared in the excited states $|ex\rangle$ and emit single photons with frequencies of either ω_1 or ω_2 . The atom and photon in each arm

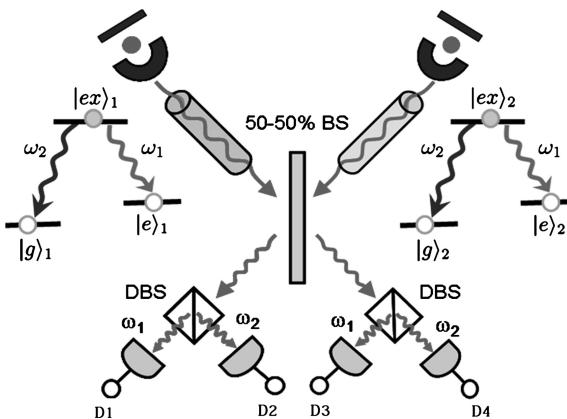


Figure 1.9 A scheme for generation of atomic entangled states by simultaneous detection of two single photons, similar to [17]. Kaoru Sanaka.

become entangled:

$$|\phi\rangle_1 = \frac{1}{\sqrt{2}}(|g\rangle_{\text{atom1}}|\omega_2\rangle_{\text{photon1}} + |e\rangle_{\text{atom1}}|\omega_1\rangle_{\text{photon1}}) \quad (1.13)$$

$$|\phi\rangle_2 = \frac{1}{\sqrt{2}}(|g\rangle_{\text{atom2}}|\omega_2\rangle_{\text{photon2}} + |e\rangle_{\text{atom2}}|\omega_1\rangle_{\text{photon2}}) \quad (1.14)$$

We assume that the photons 1 and 2 are pair-wise indistinguishable. Then, if the two single photons are recombined by a 50–50 beam-splitter and if two photons with different frequencies are simultaneously detected in the same output port of the beam-splitter, that is, $D1$ and $D2$ simultaneously click or $D3$ and $D4$ simultaneously click, the two atomic states are projected onto $|\phi\rangle_{\text{atom}} = \frac{1}{\sqrt{2}}(|g\rangle_{\text{atom1}}|e\rangle_{\text{atom2}} + |e\rangle_{\text{atom1}}|g\rangle_{\text{atom2}})$. On the other hand, if the two photons are simultaneously detected in different output ports, that is, $D1$ and $D4$ simultaneously click or $D2$ and $D3$ simultaneously click, the two atomic states are projected onto $|\phi\rangle_{\text{atom}} = \frac{1}{\sqrt{2}}(|g\rangle_{\text{atom1}}|e\rangle_{\text{atom2}} - |e\rangle_{\text{atom1}}|g\rangle_{\text{atom2}})$. Since the two detected photons have similar frequencies, $|\omega_1 - \omega_2| \ll \omega_1, \omega_2$, fiber phase fluctuation is also suppressed in this scheme.

1.4

History of Single-Photon Generation

If we include photons of any energy, the earliest experiments involving *heralded* single-photon generation date back to the early twentieth century. By ‘heralded,’ we mean that emission of a single photon is correlated in time with emission of one or more additional particles. Although the time at which a particular photon is emitted cannot be controlled, it can be known through detection of the correlated particle. Coincidence experiments involving high-energy photons (X-rays or γ -rays) are described, for example, in [18]. Correlated photon-pair emission through positron decay is the basis for positron emission tomography, demonstrated in the 1950s [19, 20].

At optical frequencies, correlated photons were first produced by atomic cascades [21] starting in the 1960s and by spontaneous parametric down conversion (SPDC) [22] beginning in 1970. Such sources were used in landmark quantum optics demonstrations such as violation of Bell’s inequality [23] and two-photon interference [24]. Over the past two decades, SPDC-based sources have continued to improve and have been used in numerous quantum optics and quantum information experiments.

The first demonstration of *photon anti-bunching* at optical frequencies was performed in 1977 using a beam of sodium atoms excited by a continuous-wave dye laser [25]. Ten years later, a similar demonstration was performed using single trapped ions [26]. This later experiment was a significant advance in that a single ion could be held in place for ~ 10 min, and the photon statistics were truly sub-Poissonian. Among solid-state systems, the first demonstration of photon

antibunching was performed in 1992 using single dye molecules embedded in a solid [27], and antibunching was later observed in nitrogen-vacancy centers in diamond [28] and in CdSe quantum dots [29]. Since all of these experiments used continuous excitation, the timing of the emitted photons was not controlled.

The first “on-demand” source of light with sub-Poisson statistics was probably one based on squeezing, demonstrated in 1993 [30], though the deviation from Poisson statistics was small. An on-demand source based on pulsed excitation of single molecules was claimed in 1996 [31]. The first demonstration that included a measured photon correlation histogram ($G^{(2)}(\tau)$) was published in 1999 [32]. In this experiment, a single molecule was rapidly swept through resonance with a continuous-wave laser by means of an applied electric field. Also in 1999, an electrically-driven semiconductor device based on Coulomb blockade was reported for which single-photon generation was claimed on the basis of electrical characteristics and timing of the emitted light [33]. Soon afterward, on-demand generation of single photons, including measurement of the photon statistics, was achieved in semiconductor quantum dots [34–36]. At around the same time, stable, triggered single-photon generation at room temperature was achieved with single molecules [37] and in nitrogen-vacancy centers in diamond [38]. An electrically-pumped device based on quantum dots was also demonstrated [39].

Following these demonstrations, attention turned toward improving the efficiency and spectral characteristics for applications such as quantum key distribution and single-photon-based quantum computation. Semiconductor quantum dots are a natural choice for integration into micron-sized optical cavities. The first significant gains in performance were reported using distributed-Bragg-reflector micropillar cavities incorporating InAs quantum dots. Such structures were used to generate single photons with enhanced photon collection efficiency [40–42]. Consecutive photons emitted by such devices were also shown to have a high degree of quantum-mechanical indistinguishability [6, 43, 44] as demonstrated in Hong–Ou–Mandel-type two-photon interference experiments using single photons produced by spontaneous emission. Photons with a high degree of indistinguishability were also produced by an electrically-pumped device [45]. Most recently, it was shown that for quantum dots embedded in quantum wells, two dots that initially had widely separated optical transition frequencies could be tuned into mutual resonance, and some degree of photon indistinguishability was observed [46].

New attention has also focused on single-photon generation with single atoms and ions. Some early results with atoms included triggered single-photon generation using three-level atoms coupled to a cavity [47] and studies of two-photon interference from this and other atomic sources [48, 49]. With trapped ions, generation of single photons with arbitrary waveforms was demonstrated [50] as well as two-photon interference of single photons emitted by two different trapped ions [51]. This work led to the first demonstration of probabilistic entanglement formation between two distant ions through photon interference and detection [52].

At present, the most compelling applications for single-photon generation appear to be for quantum communication between matter qubits, either for repeaters or for scalable computation. Much of the current effort in this field is

devoted to demonstrating a high-quality single-photon source coupled to a matter qubit with a long coherence lifetime. At present, among atom-like systems operating at optical frequencies, trapped ions have made the most progress in this area, as noted above. Nevertheless, several solid-state systems, including semiconductor quantum dots, nitrogen-vacancy centers in diamond, and shallow donors and acceptors in semiconductors also appear promising. In semiconductor quantum dots, a Λ -type three-level system involving a single electron spin can be obtained by applying a transverse magnetic field to a quantum dot containing a single electron. Some recent progress in this system includes optical spin initialization with high fidelity [53, 54], arbitrary all-optical single-qubit gates [55], and generation of photons from a single quantum dot through Raman scattering [56]. In nitrogen-vacancy centers, the electron spin coherence lifetimes are much longer [57] and controlled electron-nuclear coupling has been achieved [58, 59], but the optical transitions are weaker. A Λ -type three-level system has been demonstrated [60] and an intensive effort is underway by several groups to develop optical structures that could enable efficient stationary-to-flying qubit conversion in this system [61–71]. In shallow donors and acceptors in semiconductors, single-photon generation [72], a Λ -type system [73], all-optical spin rotation [74], and indistinguishable photons from two separate impurities [75] have recently been reported.

Numerous other atom-like systems in solids operating at optical frequencies have also been or continue to be investigated for quantum-optical applications, such as carbon nanotubes [76] and organic dye nanocrystals [77]. Continued progress has also been made with single molecules, including an experiment demonstrating the ability to tune two molecules with transform-limited spectral lines into mutual resonance [78] and most recently, a demonstration of indistinguishable photon generation from two different molecules [79]. In diamond, hundreds of optically active defects exist [80]. Some have been identified as bright, room-temperature single-photon sources [81–85], though at room temperature, the photon bandwidth is large compared with the inverse lifetime. Some of these defects could have multiple spin sublevels in the ground state with long coherence times similar to the nitrogen-vacancy center, though this is not yet known since these other defects have not been studied in such great detail. The situation remains that an ideal artificial atom possessing a combination of long-lived matter qubit coherence, strong optical transitions, and a high degree of reproducibility (e.g., small inhomogeneous broadening of the optical spectrum) has not yet been found. Therefore, there is a strong motivation to keep searching for such a system.

Extremely promising results have also been achieved recently in the microwave regime using superconducting qubits and so-called “circuit QED”. Because of the very strong coupling that can be obtained between a Josephson junction device and a superconducting strip line resonator, such devices can operate in an extreme strong-coupling regime, and reversible coupling between a photon in a transmission line cavity and a superconducting qubit has been demonstrated [86, 87]. Furthermore, these devices can be engineered and fabricated repeatedly. One limitation at present is that it is not useful to send such single photons outside of a

dilution refrigerator because of the much larger thermal photon numbers present at microwave frequencies. Nevertheless, for scalable quantum computation, this approach is one of the most promising so far.

1.5

Outline

In this book, we have chosen to focus on single-photon generation at *optical* frequencies using solid-state atom-like systems. We shall start by presenting the basic theory of single-photon generation in two-level and three-level systems in Chapters 2 and 3, respectively. In Chapter 4, we present some theoretical models for dephasing, and in Chapter 5, we briefly discuss experimental issues. In Chapter 6, we describe three solid-state atom-like systems: InAs quantum dots, nitrogen-vacancy centers in diamond, and shallow donors (or acceptors) in semiconductors. In Chapter 7, we describe various types of microcavities that can be used to enhance and efficiently collect spontaneous emission from these systems. In Chapter 8, we give some additional examples of possible applications for single-photon sources.

